U.S. ARMY COMBAT CAPABILITIES DEVELOPMENT COMMAND
CHEMICAL BIOLOGICAL CENTER
ABERDEEN PROVING GROUND, MD 21010-5424

CCDC-CBC-TR-1575

Infrared Spectroscopic Characterization of Five Variants of Pinacolyl Methylphosphonofluoridate (GD)

Barry R. Williams
Melissa S. Hulet

LEIDOS, INC.
Abingdon, MD 21010-0068

Clayton S.C. Yang

BATTELLE MEMORIAL INSTITUTE
Aberdeen, MD 21001-1228

Alan C. Samuels
Ronald W. Miles, Jr.

RESEARCH AND TECHNOLOGY DIRECTORATE

June 2019

Disclaimer

The findings in this report are not to be construed as an official Department of the Army position unless so designated by other authorizing documents.

REPORT DOCUMENTATION PAGE

Form Approved
OMB No. 0704-0188

1. REPORT DATE *(DD-MM-YYYY)*	**2. REPORT TYPE**	**3. DATES COVERED** *(From - To)*
XX-06-2019	Final	Jul 2011–Jun 2014

4. TITLE AND SUBTITLE
Infrared Spectroscopic Characterization of Five Variants of Pinacolyl Methylphosphonofluoridate (GD)

5a. CONTRACT NUMBER

5b. GRANT NUMBER

5c. PROGRAM ELEMENT NUMBER

6. AUTHOR(S)
Williams, Barry R.; Hulet, Melissa S. (Leidos); Yang, Clayton S.C. (Battelle); Miles, Ronald W., Jr.; and Samuels, Alan C. (CCDC CBC)

5d. PROJECT NUMBER
CA09DET503H

5e. TASK NUMBER

5f. WORK UNIT NUMBER

7. PERFORMING ORGANIZATION NAME(S) AND ADDRESS(ES)
Director, CCDC CBC, ATTN: FCDD-CBR-PD, APG, MD 21010-5424
Leidos, Inc.; 3465 Box Hill Corporate Center Drive, Abingdon, MD 21009-1261
Battelle Memorial Institute; 1204 Technology Drive, Aberdeen, MD 21001-1228

8. PERFORMING ORGANIZATION REPORT NUMBER
CCDC CBC-TR-1575

9. SPONSORING / MONITORING AGENCY NAME(S) AND ADDRESS(ES)
Defense Threat Reduction Agency, Joint Science and Technology Office, 6801 Telegraph Road, Alexandria, VA 22310-3398

10. SPONSOR/MONITOR'S ACRONYM(S)
DTRA JSTO

11. SPONSOR/MONITOR'S REPORT NUMBER(S)

12. DISTRIBUTION / AVAILABILITY STATEMENT
Approved for public release: distribution unlimited.

13. SUPPLEMENTARY NOTES
U.S. Army Combat Capabilities Development Command Chemical Biological Center (CCDC CBC) was previously known as U.S. Army Edgewood Chemical Biological Center (ECBC).

14. ABSTRACT
Five variants of pinacolyl methylphosphonofluoridate (GD) were analyzed in the mid-infrared region using a combination of variable-angle spectral ellipsometry and high-resolution vapor-phase spectroscopy. We report the complex optical constants ($\hat{n} = n + \mathrm{i}k$; where ^ denotes a complex quantity, n is the real part of the refractive index, and ik is the imaginary refractive index) of all five variants, as well as the effects of impurities on the vapor-phase spectra of the effluent from two weapons-grade samples. The data showed that volatile impurities in chemical agents can influence the resulting vapor-phase spectra in a manner that is out of proportion to the concentrations of the impurities in the agent, whereas the impact of the impurities on the liquid-phase spectra may be much smaller.

15. SUBJECT TERMS
Refractive index
Absorption index
Pinacolyl methylphosphonofluoridate (GD)
Fourier transform infrared (FTIR)
Infrared variable-angle spectral ellipsometry (IR-VASE)
Vapor phase
Liquid phase
Nerve agent
Complex optical constant
Infrared

16. SECURITY CLASSIFICATION OF:			**17. LIMITATION OF ABSTRACT**	**18. NUMBER OF PAGES**	**19a. NAME OF RESPONSIBLE PERSON**
a. REPORT	**b. ABSTRACT**	**c. THIS PAGE**			Renu B. Rastogi
U	U	U	UU	46	**19b. TELEPHONE NUMBER** *(include area code)* (410) 436-7545

Standard Form 298 (Rev. 8-98)
Prescribed by ANSI Std. Z39.18

Blank

PREFACE

The work described in this report was performed under project number CA09DET503H. This work was started in July 2011 and completed in June 2014. At the time this work was performed, the U.S. Army Combat Capabilities Development Command Chemical Biological Center (CCDC CBC) was known as the U.S. Army Edgewood Chemical Biological Center (ECBC).

The use of either trade or manufacturers' names in this report does not constitute an official endorsement of any commercial products. This report may not be cited for purposes of advertisement.

This report has been approved for public release.

Acknowledgment

The authors thank the late Dr. Ngai Wong (Defense Threat Reduction Agency, Joint Science and Technology Office; Alexandria, VA) for his support and encouragement of this work.

Blank

CONTENTS

FIGURES

TABLES

Blank

INFRARED SPECTROSCOPIC CHARACTERIZATION OF FIVE VARIANTS OF PINACOLYL METHYLPHOSPHONOFLUORIDATE (GD)

1. INTRODUCTION

The standoff detection communities have a continuing need for data regarding the interactions of chemical and biological warfare agents and related materials in the infrared (IR) region of the electromagnetic spectrum. For liquids, the complex parameter ($\hat{n} = n + \mathrm{i}k$) and the index of refraction (where ^ in this case denotes a complex quantity, n is the real part of the refractive index, and ik is the imaginary refractive index) describe the responses of these materials to external optical (electromagnetic) fields.[1] For pure materials in the liquid phase, the linear absorptivity coefficient, K, provides a way of identifying and quantifying those materials through a linear Beer's law relationship:

$$A = KCL \tag{1}$$

where C is concentration (in this case, volume fraction), L is path length, and A is absorbance ($\log_{10}$), which describes the degree to which the signal is attenuated by the contaminant.[2] We have previously reported the vapor-phase absorptivity coefficients of various chemical warfare agents and related materials.[3–13] The complex optical constants

$$\hat{n} = n + \mathrm{i}k \tag{2}$$

represent the optical properties of a material in terms of how an electromagnetic wave will propagate in the material, where the following apply:

- The value n, the real part of the refractive index, is related to the phase change of the applied electromagnetic field due to the interaction of light with the material.
- The value ik, the imaginary part of the refractive index, is proportional to the degree to which the applied electromagnetic field is attenuated (via absorption) by the material.When not used in the form of eq 2 to denote the imaginary part of the refractive index, the absorption index should be shortened to k, in compliance with guidelines from the International Union of Pure and Applied Chemistry (IUPAC). In those guidances, k is defined as the absorption index,[14] and hereafter, we use k to denote the absorption index.

We have reported the complex optical constants of a number of chemical warfare agents and other related materials.[15]

Spectral libraries or databases are typically populated with spectra that were obtained from high-purity materials. When the library is presented with an unknown material of similar high purity, and a representative spectrum of the unknown is included in the library, the unknown material may be successfully identified using various different algorithms. If the optical constants of the materials were recorded in the library, the intensity of the reflected and transmitted light through the liquid or vapor can be predicted accurately.

On the other hand, the presence of impurities in an unknown material can degrade the ability of a sensor to identify and quantify the unknown. In the case of a typical so-called "weapons-grade" chemical agent, impurities often include residual precursors, solvents, and byproducts of synthesis reactions. Differences in volatility between the impurities and the target compounds can cause large differences in the rates at which they transition from the liquid to the vapor phase. This means that the composition of the liquid phase of an agent (e.g., from large droplets on a surface or suspended aerosols) can differ greatly from that of the vaporized material. We have shown that in some cases, the spectral features from the impurities effectively mask the presence of the chemical agent or other target compound from a sensor that is programmed to detect only the presence of the primary target compound.[12,13] The goal of this study was to compare liquid- and vapor-phase spectra of GD variants, from cruder "weapons-grade" to highly purified reference-grade materials, and relate the spectra to the compositions of the materials. An additional goal, which was not addressed for this report, was to identify potential improvements in sensor algorithms.

Herein, we compare the GD spectra from five different samples, including two high-purity, reference-grade and three representative weapons-grade samples.

2. EXPERIMENTAL SECTION

2.1 Quantitative Vapor-Phase Fourier Transform Infrared (FTIR) Spectroscopy

The system used to acquire vapor-phase IR spectra of the GD samples incorporated a saturator cell technique to generate continuous vapor streams, which were plumbed to a multipass White cell installed in a Bruker Optics (Billerica, MA) model IFS/66V FTIR spectrometer. The spectra in this report were acquired with a HgCdTe detector. The interferograms were recorded from 15798 to 0 cm^{-1} with a 0.5 cm^{-1} resolution. Absorbance (log base 10) spectra were processed with boxcar apodization and were 2× zero-filled to obtain a data spacing of 0.25 cm^{-1}. The instrument was equipped with a variable-path White cell. In the experimental data, a path length of 2.727 m was used. Data were acquired at a speed of 60 kHz using the HgCdTe detector. Single-beam spectra of the chemical warfare agent were compared with spectra of clean, dry nitrogen, and ratios were produced. Interferograms were processed using the Bruker Optics proprietary OPUS nonlinearity correction function. All interferograms were archived to enable additional post-processing of data in the event that it was needed.

The vapor-generation system and the procedures used to generate high-resolution vapor-phase absorptivity coefficients of target compounds are documented extensively in many technical reports and conference proceedings.[3–11] The procedures used to acquire and process multicomponent spectra (i.e., from impure agents) are described in more detail in other reports.[12,13]

2.2 Vertical IR Attenuated Total Reflection Variable-Angle Spectral Ellipsometer (ATR-VASE)

Complex optical constants of the materials were measured using an IR ATR-VASE system manufactured by J.A. Woollam Co. (Lincoln, NE). The instrument consists of an IR light source; an MB102 spectrometer (ABB Bomem; Zurich, Switzerland); a pair of linear polarizers and a compensator; a high-precision, θ to 2θ sample rotational stage; and an IR detector. Plane-polarized light is reflected from the sample surface to produce elliptically polarized reflected light. Data is returned in the form of the ellipsometric parameters Ψ and Δ.

All spectra were acquired with the ellipsometer operated in ATR mode using liquid cells that incorporated 45° ZnSe internal reflection elements (IREs). The cells, which were designed and fabricated at the U.S. Army Edgewood Chemical Biological Center (ECBC; now known as the U.S. Army Combat Capabilities Development Command Chemical Biological Center; Aberdeen Proving Ground, MD), incorporate a poly(tetraflouroethylene) O-ring to provide a leak-tight seal between the IRE and the cell body. Procedures for leak checking, liquid-cell filling, and measuring and processing Ψ and Δ to generate the optical constants were reported previously.[15,16]

The instrument settings and other measurement parameters are listed in Table 1. Some earlier data[15] were recorded with the bandwidth set to 0.02 μm and the minimum intensity ratio set to a variable 2 to 5. Those settings smoothed the appearance of the spectra; however, they also varied the data spacing, generally at frequencies greater than 1600 cm^{-1}. As a result, *n* and *k* spectra had to be interpolated to 2 cm^{-1} to be compatible with spectroscopy programs that prefer evenly spaced data. Setting the bandwidth and minimum intensity ratio to zero eliminated the need to interpolate the data. All raw data files were archived to a network shared drive, which enabled additional post-processing as needed.

Table 1. Instrument Parameters Used in Ellipsometry Measurements

Parameter	Value
Resolution	4 cm^{-1}
Zero fill	2
Final data spacing	2 cm^{-1}
Spectra/revolution	15
Scan/spectrum	20
Measure/cycles/angle	10
Bandwidth	0.0 μm
Minimum intensity ratio	0
Sample type	Isotropic
Input polarizer	45° with zone averaging
RCE analyzer	Single position

2.3 Compound Details

The symbol, names, structure, and Chemical Abstracts Service Registry Number (CAS RN) for GD, the chemical agent reported on herein, are listed in Table 2. Physical properties of the compound are shown in Table 3. The data in Table 3 were extracted from U.S. Army field manual FM 3-11.9.[17]

Table 2. GD: Chemical Agent Studied for This Report

Symbol	Chemical Names	Structure	CAS RN
GD	Pinacolyl methylphosphonofluoridate 1,2,2-Trimethylpropyl methylphosphonate Soman EA-1210	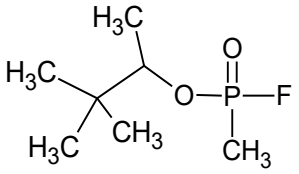	96-64-0

Table 3. Physical Properties of GD[17]

Physical Property	Value
Chemical formula	$C_7H_{16}FO_2P$
Formula weight	182.18
Density at 25 °C	1.022 g/cm^3
Vapor pressure at 25 °C	5.35 Pa

All samples were obtained from the ECBC Chemical Transfer Facility. Two of the five variants that were studied for this work were of Chemical Agent Standard Analytical Reference Material (CASARM) grade. Certificates of analysis (CoAs) were available for the two CASARM-grade samples. Each CoA included results of analysis by titration, nuclear magnetic resonance (NMR) spectroscopy, and gas chromatography–mass spectrometry (GC–MS). Two additional non-CASARM-grade samples were analyzed via GC–MS by Mr. Kenneth Sumpter (Chemistry Division, ECBC). A fifth sample, thickened GD (TGD)-U-8148-CTF-N, was prepared by adding thickener to the CASARM-grade lot GD-U-8141-CTF-N. To our knowledge, no additional analysis of sample TGD-U-8148-CTF-N was performed beyond that listed in the CoA for lot GD-U-8141-CTF-N. More detailed information about the lot numbers and chemical compositions of the variants is provided in Table 4.

Table 4. Lot Numbers and Chemical Compositions of GD Variants Studied for This Work

Lot Number	Composition*	Remarks
GD-S-0167-CTF-N	GC–MS (area %) Isopropyl isocyanate: 0.11 Isopropyl methylphosphonofluoridate (GB): 0.14 Diisopropylcarbodiimide (DICDI): 0.13 GD: 94.17 Diisopropylurea: 1.75	Non-CASARM grade; compounds listed in order of elution on a nonpolar column
GD-U-2323-CTF-N	Titration (mass %) GD: 98.8 GC–MS (area %) Isopropyl isocyanate: 0.1 GB: 0.3 DICDI: 0.9 Methylpentyl phosphonofluoridate: 0.3 GD: 97.6 Diisopropyl methylphosphonate: 0.1 Pinacolyl ethylphosphonofluoridate: 0.1 Pinacolyl propylphosphonofluoridate: 0.1 Multinuclear NMR (mol %) GD: 98.8 Other phosphonofluoridates: 0.3 Pinacolyl methylphosphonic acid: 0.1 DICDI/diisopropylurea: 1.0	CASARM grade; compounds found by GC–MS analysis were probably listed in order of elution, although this could not be verified
GD-S-5134-CTF-N	Titration (mass %) GD: 98.5 GC–MS (area %) GD: 99.1 GB: 0.21 DICDI: 0.14 ^{31}P NMR (mol %) GD: 99.2 Alkyl methylphosphonofluoridates: 0.32 Other nonchiral phosphorous: 0.25 Other P–F acids and esters: 0.10	CASARM grade; compounds found by GC–MS analysis are listed in order, from highest to lowest area fraction
TGD-U-8148-CTF-N	No additional analysis of lot was available	Prepared by thickening GD-U-8141-CTF-N

*Only those compounds that were observed at fractions ≥0.1% (using the respective technique) are reported here.

3. RESULTS AND DISCUSSION

3.1 Complex Refractive Index

3.1.1 CASARM-Grade GD

The complex refractive indices of the two CASARM-grade GD samples are shown in Figure 1. The *n* and *k* from the two lots were so similar that the plots are stacked rather than overlaid. The difference spectra (shown in the bottom row of the figure) were computed by mathematically subtracting each data point in GD-U-8141-CTF-N from the corresponding data point in GD-U-2323-CTF-N. The difference spectra exhibited little obvious patterning. The difference in the *k* spectra within the range of 2450–2350 cm^{-1}, for example, was similar to the root-mean-square (rms) noise in the region (0.0003–0.0004). The plot of the difference in the spectra of the real refractive index exhibited a small monotonic increase from low to high frequencies. Near 600 cm^{-1}, the difference in *n* was close to zero and nearly indistinguishable from noise, whereas near 4000 cm^{-1}, *n* was 1.394 for GD-U-2323-CTF-N and 1.392 for GD-U-8141-CTF-N.

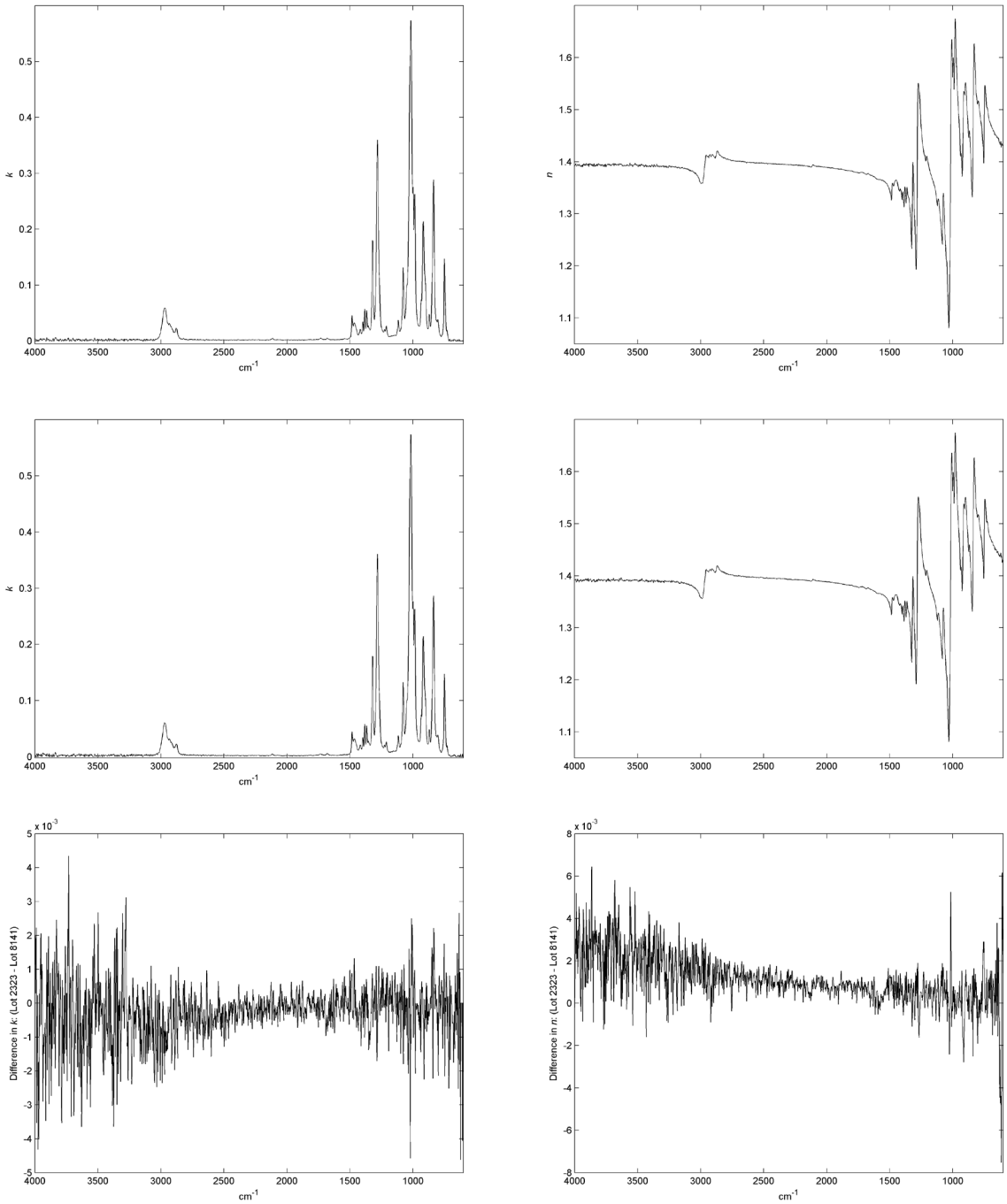

Figure 1. Complex refractive index of CASARM-grade GD. (Top row) GD-U-2323-CTF-N; (middle row) GD-U-8141-CTF-N; (bottom row) difference spectra, which were obtained by mathematically subtracting each data point in GD-U-8141-CTF-N from the corresponding data point in GD-U-2323-CTF-N. The resulting difference spectra were similar in magnitude to the rms noise, which for the *k* spectrum was approximately 0.0003–0.0004 around 2350 cm^{-1}, and little patterning was evident. At 3998 cm^{-1}, *n* was 1.394 for GD-U-2323-CTF-N and 1.392 for GD-U-8141-CTF-N.

As noted previously, both parts of the complex refractive index were obtained directly from the ellipsometric parameters in a single run. Traditional methods of measuring the complex refractive index of chemical agents involved using transmission spectra obtained with liquid cells, from which k was derived, and a Kramers–Kronig (K–K) transformation was used to compute n from k:[18]

$$n(\nu_i) = \frac{2}{\pi} P \int_0^{\infty} \frac{\nu k(\nu)}{\nu^2 - \nu_i^2} d\nu + n(\infty) \quad (3)$$

Although ellipsometry eliminates the need for the K–K transformation, and thereby also negates the need to extrapolate a value of $n(\infty)$ outside of the measured range, we found that a K–K transformation can nevertheless be useful for evaluating the internal consistency of the real refractive index that was computed directly from the ellipsometric parameters. Figure 2 shows plots of the real refractive index of the two CASARM-grade GD samples derived from Ψ and Δ, as well as n that was computed from a K–K transformation using $n(\infty) = 1.405$ (reported at 589.3 nm and 20 °C, with an uncertainty of 0.002).[18] The spectra of n that were computed from the K–K transformations were very similar to those computed from the ellipsometric parameters, and only a small scalar offset occurred at frequencies greater than 800 cm^{-1}. At 3998 cm^{-1} in the real refractive index of GD-U-2323-CTF-N, for example, n was 1.3935 versus 1.3978 for K–K, which represents a scant 0.3% difference. For GD-U-8141-CTF-N, the difference was also 0.3%: 1.3922 versus 1.3968 for the K–K transformation. Larger deviations in the traces at wavenumber (ν) < 800 cm^{-1} are an inherent limitation in the K–K transformation, which must assume that $k = 0$ outside of the measured range. Although k is likely very close to zero for ν > 4000 cm^{-1}, medium to strong absorption features are frequently observed for ν < 800 cm^{-1}. This induces a rather sharp deviation in the n that was derived from the K–K transformation vis-à-vis the traces of n that were obtained from the ellipsometric parameters. The latter are not similarly affected by the lack of spectral data outside of the measured range.

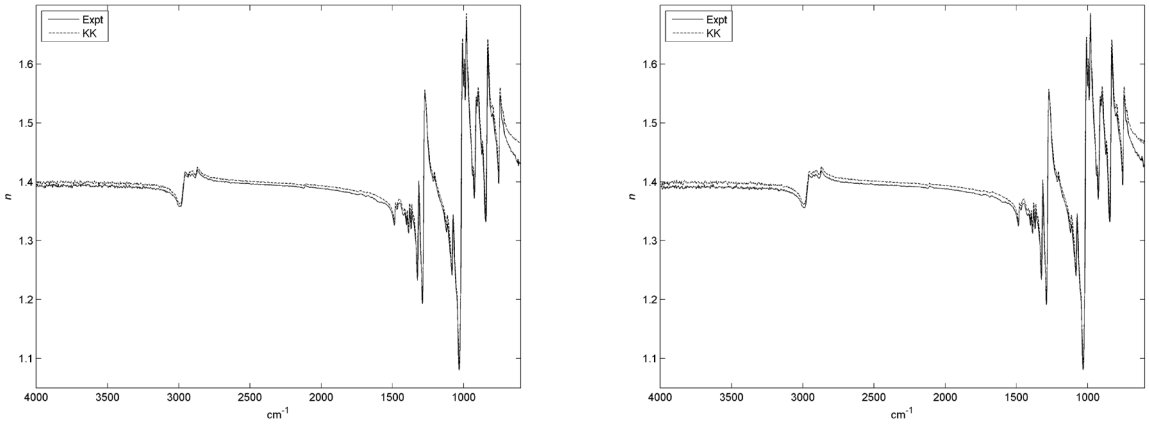

Figure 2. Values of k in the spectra of CASARM-grade GD at selected peak maxima are listed in Table 5. Intensities of the peaks in the two spectra were very similar, and the mean absolute difference was 0.0007. Values of the real refractive index at selected maxima and minima are shown in Table 6 and were similarly well matched. The mean absolute difference in the reported intensities was 0.0008.

Table 5. Positions and Intensities of Selected Peaks in *k* Spectra of CASARM-Grade GD

GD-U-2323-CTF-N		GD-U-8141-CTF-N	
cm^{-1}	*k*	cm^{-1}	*k*
750.0	0.1470	749.8	0.1473
803.2	0.0382	802.8	0.0387
837.7	0.2886	837.7	0.2863
871.0	0.0480	871.0	0.0484
918.7	0.2141	918.7	0.2145
934.2	0.0743	934.5	0.0744
986.5	0.2628	986.5	0.2629
1000.0	0.2756	999.9	0.2766
1017.5	0.5734	1017.5	0.5737
1078.5	0.1313	1078.5	0.1325
1117.6	0.0370	1117.5	0.0372
1210.5	0.0271	1210.4	0.0263
1282.4	0.3597	1282.5	0.3605
1320.2	0.1798	1320.2	0.1792
1367.2	0.0546	1367.1	0.0549
1382.5	0.0574	1382.6	0.0582
1399.0	0.0342	1398.9	0.0342
1418.3	0.0210	1418.2	0.0211
1464.7	0.0326	1463.3	0.0320
1482.6	0.0455	1482.4	0.0447
2878.8	0.0229	2877.9	0.0224
2969.5	0.0588	2970.7	0.0609

Table 6. Positions and Values of Selected Maxima and Minima in the Real Refractive Index of CASARM-Grade GD

GD-U-2323-CTF-N		GD-U-8141-CTF-N	
cm^{-1}	*n*	cm^{-1}	*n*
754.9	1.398	754.9	1.395
797.8	1.517	797.9	1.518
830.1	1.627	830.1	1.627
846.0	1.332	845.9	1.332
898.7	1.552	898.9	1.551
925.0	1.372	925.3	1.371
981.5	1.675	981.5	1.675
1008.4	1.635	1008.4	1.636
1032.2	1.080	1032.1	1.081
1074.2	1.340	1074.1	1.338
1082.8	1.241	1082.8	1.240
1273.5	1.551	1273.0	1.552
1289.7	1.193	1289.7	1.192
1315.8	1.399	1315.7	1.399
1325.5	1.233	1325.6	1.234
1363.8	1.351	1363.8	1.351
1370.6	1.320	1370.5	1.320
1378.7	1.352	1378.8	1.352
1386.6	1.313	1386.6	1.313
1396.3	1.343	1396.2	1.343
1402.3	1.327	1402.3	1.326
1414.9	1.348	1414.8	1.346
1421.9	1.343	1422.5	1.343
1487.5	1.326	1487.4	1.325
2866.1	1.421	2866.6	1.419
2884.0	1.407	2884.1	1.406
2955.7	1.413	2956.0	1.412
3998.0	1.394	3998.0	1.392

As shown in Table 4, GC–MS analysis of both CASARM-grade GD samples indicated that the area fractions of diisopropylcarbodiimide (DICDI) were 0.9% for GD-U-2323-CTF-N and 0.14% for GD-U-8141-CTF-N, and NMR analysis of GD-U-2323-CTF-N yielded a molar fraction of 1.0% of the stabilizer in that lot. We previously measured the complex optical constants of DICDI by IR ATR-VASE (Figure 3). The *k* spectrum exhibited a very intense feature at 2116 cm^{-1} with $k = 0.855$, which was presumably associated with the stretch of the coordinated double bonds (carbodiimide) in the molecule, R–N=C=N–R.[2] Because of the intensity of this vibration, the presence of the compound was readily observed in the *k* spectra of the CASARM-grade samples (Figure 4). The peak height of the feature in the GD samples was estimated to have a volume fraction of approximately 0.3–0.4%. That volume fraction was

roughly consistent with the area fraction (0.9%) that was identified by GC–MS and the molar fraction of DICDI/ureas (1.0%) that was measured by NMR. Because the CoA information for GD-U-2323-CTF-N was based upon instrumental analyses that had been performed in 1994, we consider such a close agreement to be remarkable. Based on a visual estimation of the signal-to-noise ratio of the spectrum from the ellipsometer, the feature associated with the DICDI was probably too small in both samples to support a more rigorous or precise quantitation.

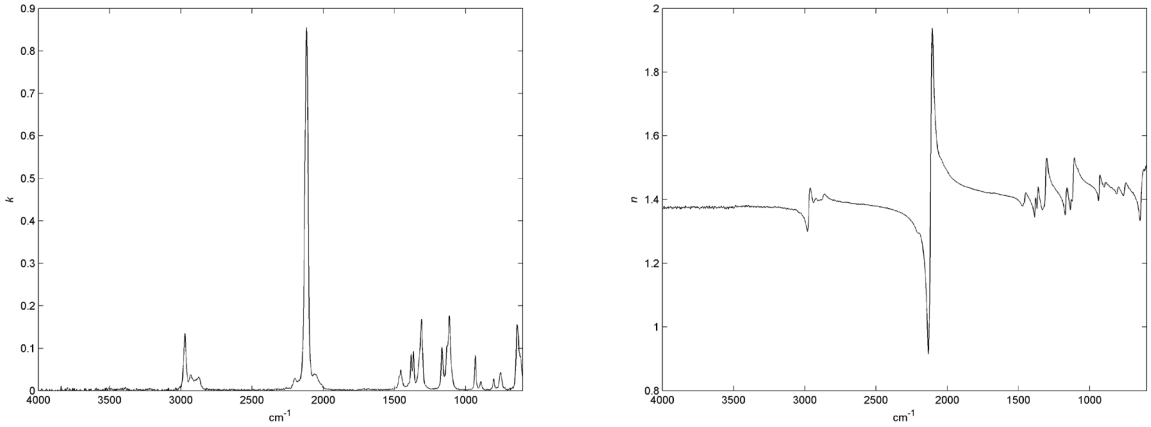

Figure 3. Complex optical constants of DICDI.

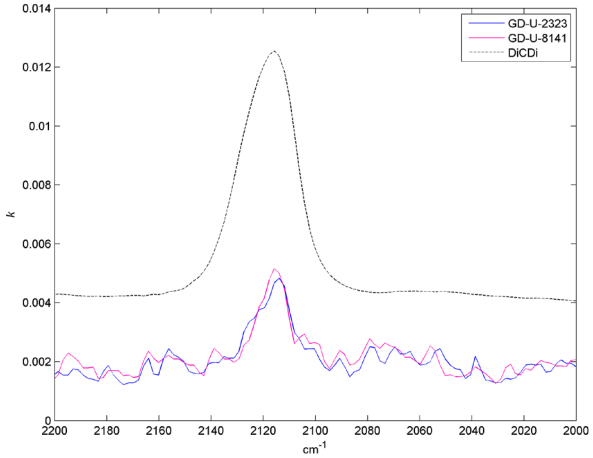

Figure 4. Imaginary refractive indices of GD-U-2323-CTF-N, GD-U-8141-CTF-N, and DICDI in the vicinity of the strong carbodiimide stretch. The presence of the absorption band associated with carbodiimide stretch in both GD samples is shown. The DICDI was scaled and offset from the spectra of the GD.

The most recent prior measurements of the GD optical constants were made by researchers from Pacific Northwest National Laboratory (PNNL; Richland, WA) at Dugway Proving Ground, UT and were reported in 2008.[18] In the earlier work, the optical constants were determined using a transmission method in liquid cells combined with a K–K transformation using $n(\infty) = 1.4068$ (with no uncertainty given). Although the method was very different from that used in our work, the PNNL measurements were coincidentally made using GD-U-2323-CTF-N. This provided us with a unique opportunity to compare two different techniques for obtaining the optical constant of a toxic chemical agent. Figure 5 shows the fingerprint region in the k spectra from the two laboratories and at 3998–601 cm^{-1} for the real refractive index. The shapes and intensities of the features in the spectra were very similar. The peak-picking algorithm in Grams/32 software (Thermo Fisher Scientific; Waltham, MA) was used to evaluate the positions and maximum intensities of the peaks in the spectrum. The positions of the 16 strongest peaks differed by an average of only 0.26 cm^{-1}. The mean difference in their intensities was 4.7%. The latter included several peaks where $k_{max} = 0.034–0.048$. The mean difference in the intensities of the 10 peaks with $k > 0.048$ was only 2.2%. Because the data spacing in the PNNL spectrum (nominally 1 cm^{-1}) differed from that in the ellipsometer spectrum (nominally 2 cm^{-1}), it was useful to compare integrated areas rather than absolute peak intensities in the two spectra. Within the range of 1500–700 cm^{-1}, the integrated intensity in the ECBC spectrum was 56.87 versus 57.59 for the PNNL spectrum. This represented a fractional difference of only 1.3%. The real refractive indices from the two laboratories were even more similar. The mean fractional difference in the values of 40 minima/maxima was a scant 0.1%. At 3998 cm^{-1}, $n = 1.3935$ (ECBC) and $n = 1.3953$ (PNNL). As noted, the real refractive index reported by PNNL was obtained through a K–K transformation, and the difference in the ECBC and PNNL n values at 3998 cm^{-1} was smaller than the range of the literature values for n at 589.3 nm.

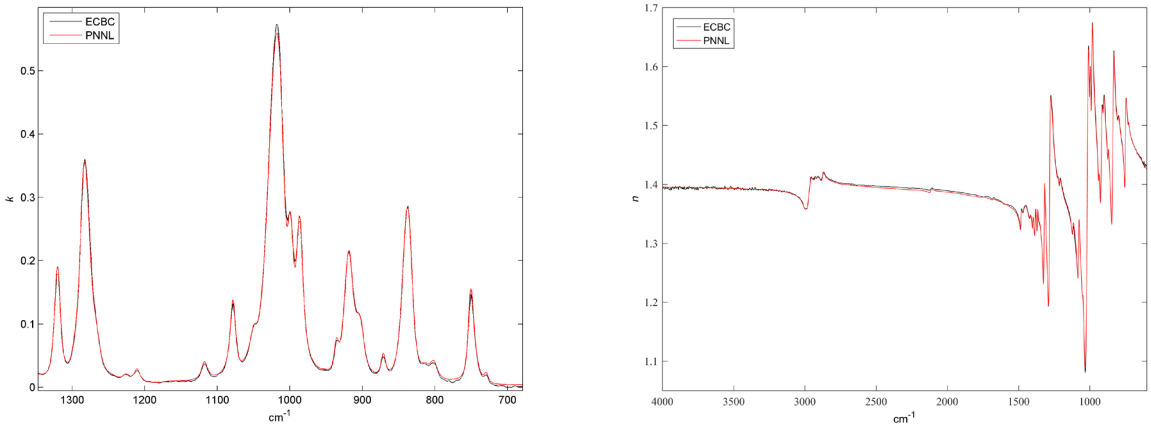

Figure 5. Complex refractive indices of GD from ECBC (blue traces) and PNNL (red traces). The positions and intensities of the peaks in the k spectra, which are expanded to the fingerprint region, and n spectra, which are shown full scale, are very similar.

3.1.2 Thickened GD

As noted in Table 4, TGD-U-8148-CTF-N was prepared by adding K-125 thickener to a CASARM-grade lot, GD-U-8141-CTF-N. The K-125 additive is a proprietary acryloid polymer with the trade name Paraloid that was manufactured by Rohm and Haas (Philadelphia, PA).[19] Thickened GD typically contains 5% (by weight) of K-125 additive.[20] According to Armor and Ogston,[21] K-125 thickener consists of the following mole fractions: 82% poly(methyl methacrylate) (PMMA), 12% poly(ethyl methacrylate), and 6% poly(isobutyl methacrylate). All three polymers are composed of alky methacrylate esters and thus share similar absorption features,[22] in particular, a very strong ester carbonyl stretch near 1730 cm^{-1}. We recently measured the optical constants of K-125 thickener. A thin film was prepared by airbrushing a solution of the polymer in 80:20 (v/v) acetonitrile/acetone onto a ZnSe prism and measuring it by IR ATR-VASE. The complex optical constants of the K-125 thickener (shown in Figure 6) are similar to those of PMMA, which we have reported previously.[23] The spectra in Figure 6 were obtained from Rohm and Haas for lot number 3-66326. Variations in average molecular weights and crystallinity can induce subtle differences in the IR spectra of polymers. For that reason, IR libraries often include multiple spectra of an individual polymer type, and the spectra differ only by their average molecular weight or crystallinity.

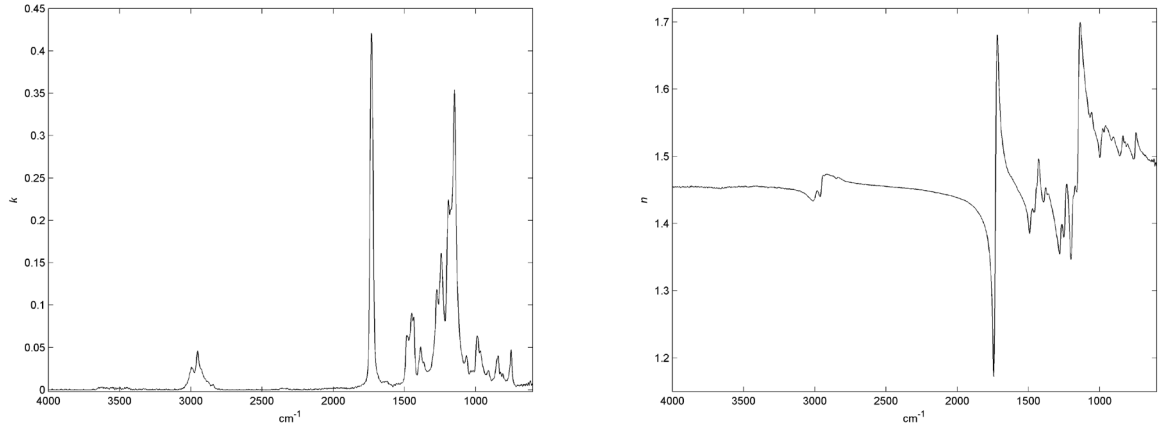

Figure 6. Complex optical constants of K-125 thickener from IR ATR-VASE measurements of an airbrushed thin film of the polymer on a ZnSe prism.

The optical constants of the thickened GD (Figure 7) were similar to those of the unthickened agent (Figure 1). The most obvious difference was a peak at 1732 cm^{-1}. Given the weakness of the feature and the unknown possible influence of intermolecular interactions between the GD and the thickener, this is remarkably similar to the position of the ester carbonyl in the thin film of the neat polymer, which was observed at 1731 cm^{-1}.

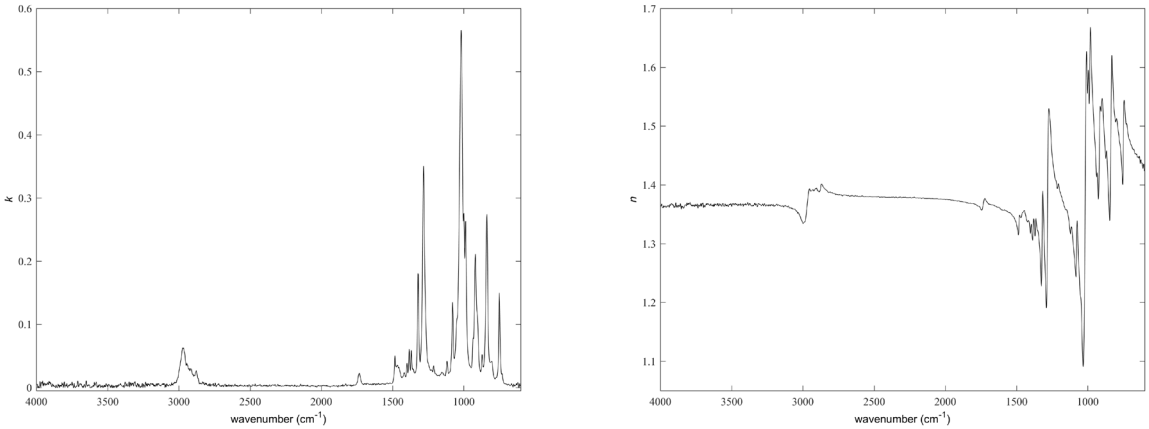

Figure 7. Complex optical constants of TGD-U-8148-CTF-N.

The absorption index can be computed from *K* as follows:

$$k(\tilde{\nu}) = \frac{\ln(10)\,K(\tilde{\nu})}{4\pi\tilde{\nu}} \tag{4}$$

If eq 1 is rewritten to put *K* on the left side of the equation,

$$K(\tilde{\nu}) = \frac{A(\tilde{\nu})}{CL} \tag{5}$$

and if *L* is to unit length (1 cm in this case), eq 5 becomes

$$K(\tilde{\nu}) = \frac{A(\tilde{\nu})}{C} \tag{6}$$

Substituting eq 6 for $K(\tilde{\nu})$ in eq 4 gives

$$k(\tilde{\nu}) = \frac{\ln(10)\,A(\tilde{\nu})}{4\pi\tilde{\nu}C} \tag{7}$$

If we ignore the factors noted above that can alter the spectra of the individual components in an admixture, eq 7 implies that, at least as a first approximation, the wavenumber-dependent absorption index of the thickened GD should be as follows:

$$k_{\mathrm{TGD}}(\tilde{\nu}) = k_{K125}(\tilde{\nu}) \times C_{K125} + k_{\mathrm{GD}}(\tilde{\nu}) \times C_{\mathrm{GD}} \tag{8}$$

Several mathematical approaches were used to estimate the influence of the thickener on the features of the thickened GD. The first, and simplest, was to subtract the baseline height in the unthickened GD, $k_{\mathrm{GD}} = 0.0043$, in the vicinity of 1730 cm^{-1}, from the $k_{\max}$ of thickened GD, 0.0210. The result, 0.0167, which was assumed to be the contribution of the thickener to the absorption index, was divided by the $k_{\max}$ of the K-125 thickener, 0.4209, yielding an initial estimate of $C_{\mathrm{PMMA}} = 0.040$. The *k* spectrum of the K-125 thickener was multiplied by the initial estimated K-125 fraction and subtracted from the k_{TGD}. The resulting residual spectrum was compared to the spectrum of the "pure" GD and was subjectively judged to be more similar to k_{GD}.

Two MATLAB (MathWorks; Natick, MA) multiple linear regression functions, *regress.m* and *robustfit.m*,[24] were then used to compute the K-125 fraction in the thickened GD, while limiting the data to points within the range of 1800–740 cm^{-1}. This minimized the influence of absorption features where k was close to zero. The previous result, $C_{PMMA} = 0.040$, was used only as a "reality check" of the results from the MATLAB computations. Of the two MATLAB programs, *regress.m* uses a simpler classical least-squares (CLS) method, in which all data points in the regression are weighted equally. In contrast, *robustfit.m* uses a more robust least-squares (RLS) fitting method that iteratively reweights data points with a bisquare function, assigning lower weights to data points that do not fit as well. The latter method may be more useful in the present situation, in which intermolecular interactions and the presence of copolymers can influence the shapes and intensities of spectral features. In fact, however, both regression functions returned similar values for the thickener fraction in the thickened GD: 0.0355 (*regress.m*) and 0.0358 (*robustfit.m*). Figure 8 shows an overlay of spectra of thickened GD and unthickened agent from lot GD-U-8141-CTF-N, as well as the result spectrum obtained by subtracting $0.358 \times k_{K125}$ from k_{TGD}. As shown in the figure, the result spectrum was very similar to the k_{GD} spectrum. Plots of the residuals from the two fitting methods are shown on the right side of Figure 8.

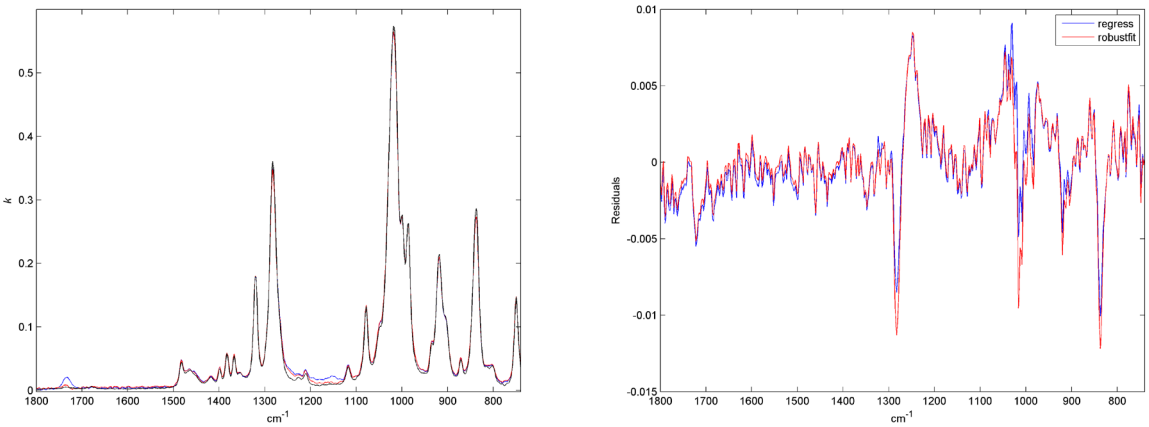

Figure 8. Least-squares estimates of the fractional contribution of K-125 polymer to k_{TGD}. Left: k_{TGD} (blue trace); $k_{TGD} - k_{K125} \times 0.0358$ (red trace); k_{GD} (black trace). Red and black traces are very similar, particularly in the region of strong C–O absorption (1200–1000 cm^{-1}). Right: Residuals from least-squares estimates of the thickener fraction in thickened GD.

In a strict mathematical sense, C represents volume fractions of the K-125 thickener and GD that are related back to the density of the pure materials in their original physical states. The specific gravity of K-125 thickener is 1.15.[19] As noted in Table 3, the specific gravity of GD is approximately 1.02. Therefore, a K-125 volume fraction of 0.0358 represents a mass fraction of: $\frac{1.15}{1.02} \times 0.0358 \approx 0.040$. This mass fraction of thickener was likely similar to that of the thickened GD as it was originally prepared.

As shown in Figures 7 and 8, at a mass fraction of <5%, the contributions of the K-125 thickener to the spectra of the thickened GD were generally subtle. Euclidean distance (ED) is a commonly used algorithm within commercial spectroscopy software for matching

unknown spectra by searching spectral libraries.[25] Mathematically, ED values can range from ED = 0, a perfect match, to ED = 1, no match. ED is implemented in the MATLAB function *pdist.m* and was used to compare the spectra of GD and thickened GD, including a thickened GD spectrum that was processed by subtracting the estimated volume fraction of PMMA, namely, $k_{TGD,corr} = k_{TGD} - k_{PMMA} \times 0.0349$. Matches were run on the spectra from the full spectral range, 3998–601 cm^{-1}, and a narrower range, 1350–700 cm^{-1}, which encompasses the strongest features in the GD. As summarized in Table 7, the results indicated that subtracting a scaled spectrum of the K-125 thickener from the thickened GD spectrum slightly improved the match. This held true for the spectra that were matched across their full spectral range as well as for the pairs that were compared within only the narrower spectral range. In any case, as also shown in Table 7, a common way of presenting the search results is to subtract the ED value from 1 and multiply the result by 100 to give, for example, a hit quality index (HQI) of 100 for a perfect match and 0 for no match.[25] An automated search algorithm, and most human operators, would generally consider all of the HQIs in Table 7 to be excellent matches. In such a case, an experienced operator will often perform a visual comparison between the unknown spectrum and the first several matches to look for subtle differences that may indicate either a slight structural difference between the unknown and the library spectra or the presence of an additional compound in the unknown.

Table 7. ED Matches between GD–Thickened GD Pairs

Spectral Pair	Range (cm^{-1})	ED	HQI*
GD–TGD	4000–601	0.0545	94.55
GD–TGD, corrected†		0.0426	95.74
GD–TGD	1350–700	0.0397	96.03
GD–TGD, corrected†		0.0243	97.57

TGD, thickened GD.
*HQI = (1 – ED) × 100.
†$k_{TGD,corr} = k_{TGD} - k_{PMMA} \times 0.0349$.

We note that the effects of impurities and additives on the spectra of chemical agents that are analyzed in the liquid state can differ greatly from vapor-phase spectra of the same lot of agent that was obtained by evaporation or purging of the liquid.[13] This was most dramatically obvious in the case of stabilized VX, with a purity of approximately 95%, that was analyzed by purging the agent with nitrogen carrier gas and acquiring spectra of the effluent over several days.[12] The resulting spectra were dominated by high-volatility species present at low concentrations in the liquid VX, whereas spectral features associated with VX vapor were largely not observed. On the other hand, the thickened GD represented nearly the opposite case: a solution composed of a nonvolatile solute, the acryloid polymer, in a much more volatile solvent, GD. As such, spectra of the vaporized effluent from the thickened GD would not be expected to differ sufficiently from those of an unthickened sample of the agent for the changes to have been observed. For that reason, the thickened agent was not run with the purged saturator cell technique.

3.1.3 Complex Refractive Index of Non-CASARM-Grade GD

The complex refractive indices of GD-S-0167-CTF-N and GD-S-5134-CTF-N are shown in Figure 9. The top row shows n and k within the full spectral range of the ellipsometry measurements, and the traces in the middle row are expanded to the fingerprint region. In the bottom row, k is expanded to show the region within 2200–1600 cm^{-1}. The spectra were similar to one another and to the spectra of the CASARM-grade agents. The k_{max} was observed at 1017.5 cm^{-1} (k = 0.557) for GD-S-0167-N and at 1017.8 cm^{-1} (k = 0.548) for GD-S-5134-CTF-N. The n_{max} was observed at 981.3 cm^{-1} (n = 1.665) for GD-S-0167-CTF-N and at 981.6 cm^{-1} (n = 1.659) for GD-S-5134-CTF-N.

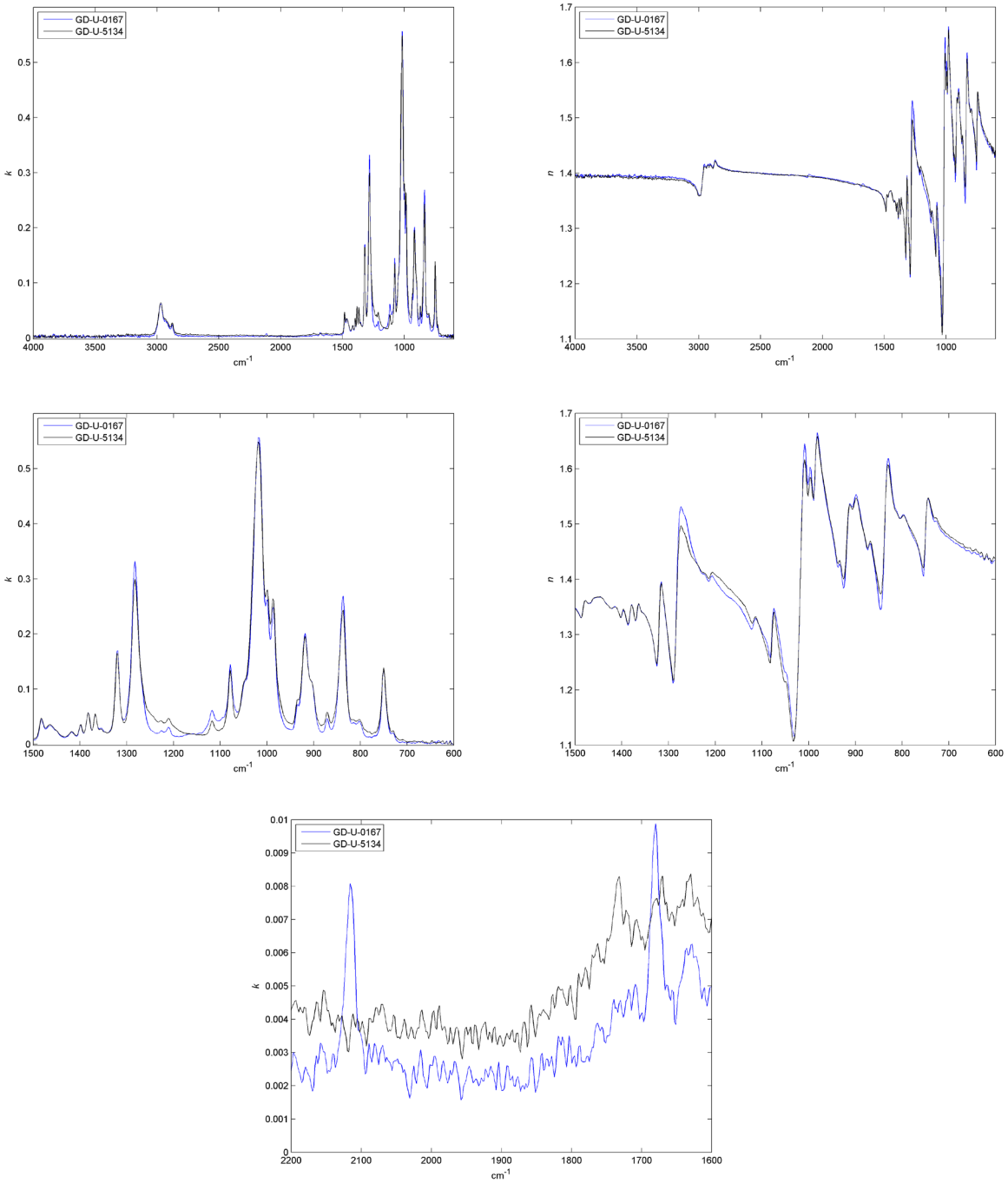

Figure 9. Complex refractive indices of GD-S-0167-CTF-N (blue traces) and GD-S-5134-CTF-N (black traces). Top row: *k* and *n* within the full range of the ellipsometry measurements. Middle row: range is expanded to the fingerprint region within 1500–600 cm^{-1}. The greatest absolute differences between the optical constants of the two non-CASARM-grade samples are seen in this region. Bottom row: plot shows peaks around 2116 cm^{-1} (DICDI) and 1680 cm^{-1} (possible diisopropylurea).

Closer examination of the spectra in the middle row of Figure 9, which are expanded to the fingerprint region, reveals differences in intensities that are most pronounced in the region between 1300 and 800 cm^{-1}. The *k* spectrum of GD-U-8141-CTF-N was used as the reference to compute the ED between the CASARM-grade and the non-CASARM-grade samples, giving ED = 0.0725 (HQI = 92.75) for GD-S-0167-CTF-N, and ED = 0.115 for GD-S-5134-CTF-N (HQI = 88.47). In this case, the sample with the lower purity as assessed by GC–MS (GD-S-0167-CTF-N) yielded the higher HQI. Although good, both matches may lead an experienced analyst to look for differences in shapes or intensities of peaks that could indicate the presence and identity of an impurity.

As explained in Table 4, the two non-CASARM-grade samples were supplied without CoAs or any other instrumental analyses of the lots. GC–MS analysis (courtesy of the ECBC Chemical Methodologies Branch) was used to determine the relative purities of the two samples that are shown in Table 4. The GD area fractions and impurities that are shown in the table were computed by integrating the peaks of the individual compounds and dividing by the summed areas of the total ion chromatograms (TICs). In this technique, it is assumed that the fragmentation patterns of individual compounds in a mixture are similar to one another and are proportional to their molar fractions. Because this method does not incorporate the use of internal or external reference standards, it provides only rough estimates of mass or molar fraction. Another limitation is that not all compounds are amenable to gas chromatography because of low volatility, thermal instability, or reactivity.

The TIC from GD-S-0167-CTF-N was populated with 15 peaks that were large enough for the peak areas to be integrated by the runtime environment (RTE) integration parameters in the MSD ChemStation software (Agilent Technologies; Santa Clara, CA). Among the impurities noted in Table 4, the largest fraction, at 1.75%, was diisopropylurea, which is the byproduct of the reaction of water with the DICDI stabilizer. The second-largest fraction after GD diester (dipinacolyl methylphosphonate), which comprised 0.78% of the TIC, was not identified. Based upon its mass spectrum and elution time, it was probably from a high-molecular-weight compound. GD diester comprised 0.59% of the TIC. Two low-molecular-weight alkenes accounted for 0.26% of the total area of the TIC. GB, which has a spectrum similar to that of GD, was observed at an area fraction of 0.14%. Peaks containing 2.65% of the total peak area in the TIC could not be assigned to a specific chemical compound. Among the impurities observed in the GC–MS analysis, to our knowledge, the only compounds for which the complex refractive indices were available were the pinacolyl alcohol (PinOH), DICDI, and GB. Despite the paucity of reference standards, an analysis of the spectrum of the stabilized agent was attempted using the RLS approach. The spectra of the GD and the PinOH, DICDI, and GB reference standards were truncated to the region of 2200–600 cm^{-1} to minimize the influence of small baseline differences in regions where $k \approx 0$. The results are summarized in Table 8. The computed volume fraction of GD (94.10%) and the volume fractions of DICDI and GB (both <0.5%) appeared reasonable. On the other hand, the computed volume fraction of PinOH, 2.68%, did not appear to be credible. The TIC from the GC–MS analysis had a peak at the retention time of PinOH, but it was too small to be integrated using the default parameters. A reason for the apparent discrepancy may be indicated in Figure 10, which shows the weights assigned by *robustfit.m* to the individual data points, along with spectra of the reference compounds (computed from 10^{-k} for display purposes only). As shown in Figure 10, unlike in

DICDI and PMMA, in which the strongest features are well separated from those of GD, the strongest absorption lines in GD, GB, and PinOH share similar spectral regions. As Figure 10 illustrates, the regions exhibiting strong absorption by GD, GB, and PinOH were strongly deweighted by the RLS fitting method. This forced the fits to use weaker absorption lines with lower signal-to-noise ratios. We concluded that in the absence of additional reference spectra of the impurities in the GD or training sets from spectra of additional lots of weapons-grade GD of known composition, the robust fit provided, at best, only a semiquantitative measure of the concentration of the impurities in the agent.

Table 8. Results from RLS Analysis of *k* Spectrum from GD-S-0167-CTF-N

Compound	Volume Fraction (%)
GD	94.10
DICDI	0.14
PinOH	2.68
GB	0.45

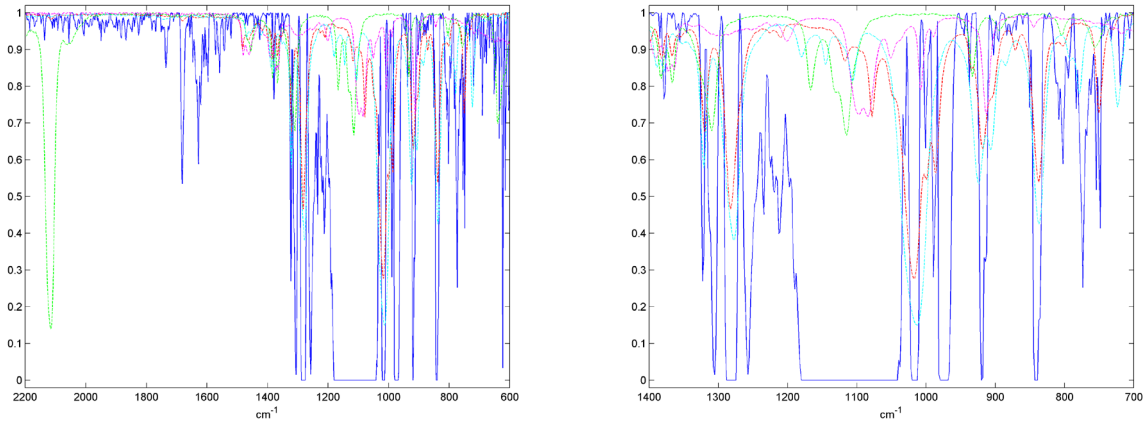

Figure 10. RLS fit of GD-S-0167-CTF-N. Blue trace shows weights assigned to individual data points in robust fit of the *k* spectrum of the sample. Dashed traces show the spectra of CASARM-grade GD (red), DICDI (green), PinOH (purple), and GB (cyan). For clarity, the reference spectra are presented in pseudo-transmission mode (10^{-k}). Many of the regions encompassing the strongest absorption lines in the reference spectra were heavily deweighted by *robustfit.m*, indicating that the spectrum of the weapons-grade GD was not well modeled by a simple linear combination of the reference spectra.

3.2 Vapor-Phase Spectra of Stabilized GD

As noted in Table 4, GD-U-2323-CTF-N was a well-characterized, high-purity CASARM-grade agent. As seen in Figure 4, the complex refractive index was generally unremarkable. Other than a trace of DICDI that was evident in both the *n* and *k* spectra, little else was observed during the analysis of the liquid by IR ATR-VASE. This made the sample useful for contrasting the differences in spectra obtained from vapor and liquid of the same lot of the agent. The GD had originally been procured with the intention of using it to acquire the vapor-phase absorptivity coefficient. However, upon acquiring vapor-phase spectra of the effluent from a saturator cell, we observed prominent absorption features from at least two impurities: DICDI and isopropyl isocyanate, the latter of which was identified on the basis of its similarity to that of the spectrum of *n*-propylisocyanate from the PNNL vapor-phase spectral library.[18]

We have previously described in more detail the theory and mathematics that illustrate the evaporation rate of individual components in a solution and the use of CLS to compute their respective concentrations.[12] The following constitutes only a brief review. According to Raoult's law, in an ideal solution, the partial pressure of a solute is proportional to the partial pressure of the pure solute and its molar fraction in the solution:[26]

$$P = PaXa + PbXb + PcXc\ldots \tag{9}$$

where *X* represents the molar concentration of the individual components in the solution. As a result of Raoult's law, the concentrations of the individual components in the headspace above a solution are rarely equal to the concentrations of those compounds in the liquid. Even high-purity chemical agents usually contain trace concentrations of precursors, byproducts, and stabilizers that are more volatile than the agent and contribute disproportionately to the vapor. Vapor-phase spectra of compounds at low concentrations in air or nitrogen are much less subject to intermolecular interactions (to include other species that may be present) that can broaden peaks and shift their positions.[27] The concentrations of the individual compounds in the vapor could be readily computed with Beer's law:[25]

$$c_i = \frac{A_i(\tilde{\nu})}{a_i(\tilde{\nu})L} \tag{10}$$

This is similar to the method that was used to analyze the impurities in the liquid phase. However, unlike what we found for the liquid-phase measurements, we observed that the response of the higher-resolution vapor-phase spectra acquired with the IFS-66 spectrometer can be very linear as long as $A_i(\tilde{\nu}) \leq 1.2$. In the past, there were few quantitative, high-resolution vapor-phase spectra of chemical weapons-related materials available. In recent years, two libraries of high-resolution vapor-phase absorptivity coefficients of chemical agents, precursors, and common impurities have been published.[3,18] Although gaps remain, it has become possible to identify and quantify a wider variety of impurities in vapor-phase spectra of chemical agents.

Figure 11 shows two views in the vapor-phase spectrum of the CASARM GD that are overlaid with reference spectra. The left side of the figure shows the region between 2500 and 2000 cm^{-1}. That region in the spectrum of GD-U-2323-CTF-N exhibits absorption bands from the coordinated double bonds in diimide (near 2130 cm^{-1}) and isocyanate (near 2270 cm^{-1}). For comparison, the reference spectrum of the DICDI in the figure, which was from the ECBC

Spectral Database, was scaled to a concentration–pathlength product (CL) of 50 µmol·mol^{-1}·m. A quantitative vapor-phase reference spectrum of isopropyl isocyanate was not available. The red trace on the left side of the figure is that of *n*-propylisocyanate, which was obtained from the PNNL database. Note that the *x* axes in the reference spectra were truncated to the regions encompassing the strong absorption from the coordinated double bonds. The right side of Figure 11 shows the fingerprint region. The reference spectrum of GD in the plot, which was taken from the ECBC Spectral Database, was scaled to a CL of 164 µmol·mol^{-1}·m, which was the approximate CL of GD-U-2323-CTF-N at the time the spectrum was acquired. The reference spectrum of DICDI in the plot on the right of Figure 11 was scaled to 120 µmol·mol^{-1}·m, which better matches the concentration of the compound in the effluent from GD-U-2323-CTF-N at the time the spectrum was acquired. Therefore, the stabilizer, which constituted a molar fraction of only approximately 1% in the liquid, was present in the vapor phase at a molar fraction that was approximately 75% that of the GD.

A partial explanation for the large difference in the concentration of the DICDI in the liquid vis-à-vis the vapor can be found in the large differences in their vapor pressures. At 22.5 °C (the temperature of the bath in which the saturator cell was suspended), the vapor pressure of GD, computed from its Antoine coefficients,[28] was 44.16 Pa. At the same temperature, the pure component vapor pressure of DICDI was 535.2 Pa.[29] If the molar fraction of DICDI is assumed to be approximately 1% (from NMR analysis), the expected partial pressure of DICDI in the liquid GD (from eq 9) is around 5.4 Pa, the predicted partial pressure of GD is 42.6 Pa, and the expected molar fraction of DICDI in the vapor is 12%. At least in our experimental setup, the GD–DICDI fluid system clearly departed from ideality, and it was necessary to determine its properties empirically.

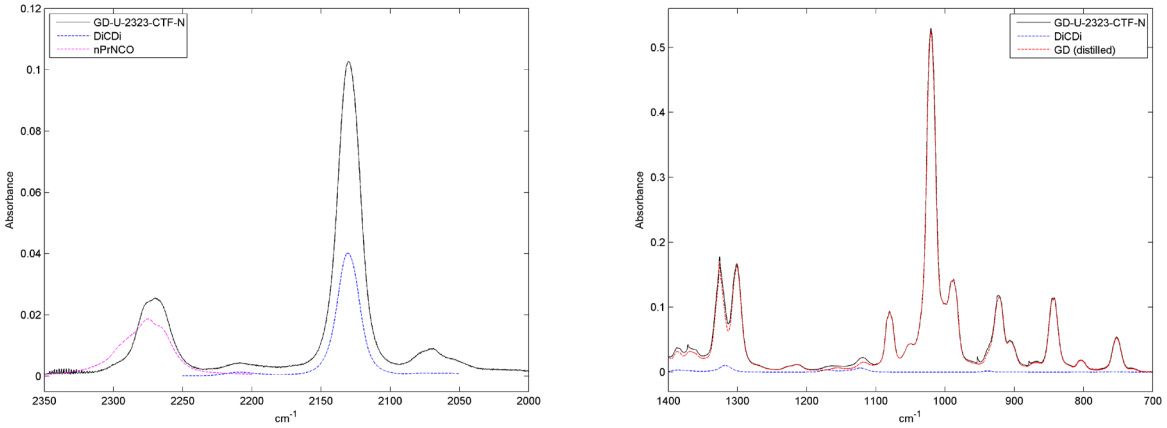

Figure 11. Vapor-phase spectra of GD-U-2323-CTF-N and scaled reference spectra. Right: plots show the scaled vapor-phase absorptivity coefficients of DICDI (120 µmol·mol^{-1}·m) and GD (164 µmol·mol^{-1}·m), which were both close to their actual CLs in the vapor from GD-U-2323-CTF-N. Although DICDI was present at a CL that was nearly 75% that of the GD, the DICDI contributed little to the spectrum of the vapor in the fingerprint region. Left: the figure is expanded to show the relatively strong contributions by the stabilizer DICDI and a presumed isocyanate impurity, which was identified by the similarity of its spectrum to *n*-propyl isocyanate. For readability only, portions of the spectra of the two impurities are shown.

The spectrum of DICDI is characterized by very strong features around 2130 cm^{-1}, which is well outside the regions in which most other organic compounds exhibit their most intense absorption bands. As shown in Figure 11 (right), even at a CL of 120 $\mu mol \cdot mol^{-1} \cdot m$, the DICDI exerted only a relatively small influence on the spectrum of the vapor from GD-U-2323-CTF-N within the fingerprint region.

As noted previously, GD-U-2323-CTF-N was originally procured to measure the vapor-phase absorptivity coefficient of GD. Carbodiimide and isocyanate impurities in the vapor stream rendered the agent not useful for that purpose. Initially, in an attempt to purge the GD, we pushed nitrogen carrier gas at a fixed rate through the saturator while we monitored the IR spectra of the effluent. At first, the DICDI fraction decreased rapidly; however, the decrease was asymptotic, and we realized after several days that it would not be practicable to remove the remaining trace fraction of the impurity. (As we subsequently discovered while analyzing the vapor effluent from weapons-grade VX, the VX–DICDI system displayed a similar behavior.[12])

Therefore, we decided to use the sample to further investigate the dynamics of the GD–DICDI system. This was accomplished by adding 95.9 mg of DICDI to the saturator cell, thereby increasing the molar fraction of DICDI to 3.55% and giving predicted partial pressures of P = 19.0 Pa for DICDI and P = 42.6 Pa for GD. When a time series of effluent spectra was obtained, the composition of the vapor was largely as expected, as shown in Figure 12.

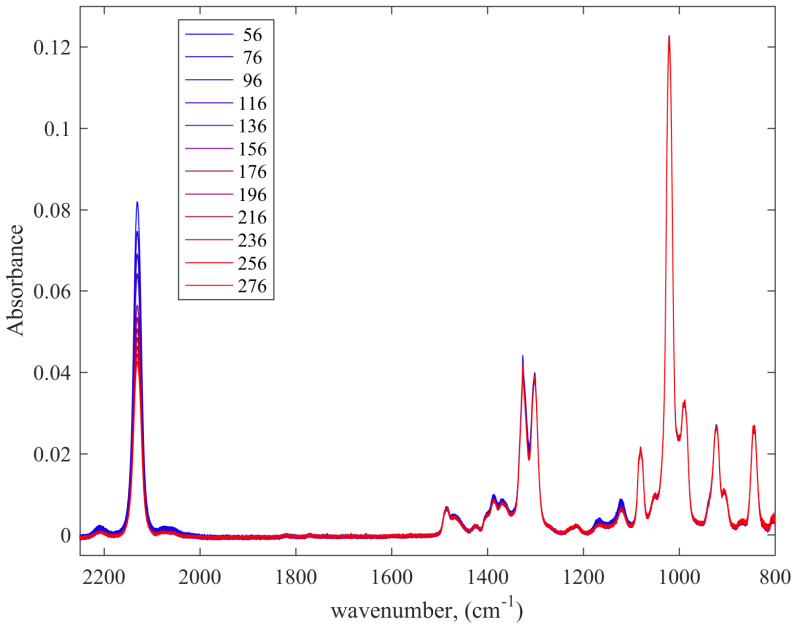

Figure 12. Series of vapor-phase IR spectra of GD from a saturator cell that had been spiked with DICDI to a molar fraction of 3.55%. The numbers in the legend indicate the time (in minutes) from the start of the carrier flow. As expected, the DICDI (indicated principally by the strong, sharp absorption band near 2130 cm^{-1}) exhibited a rapid decay.

As noted previously, the strongest absorption features in GD and DICDI were present in different spectral regions; however, there was weak interference by DICDI within the 1200–800 cm^{-1} region, where GD absorbed most strongly. For that reason, the concentrations of DICDI and GD in the vapor were computed with MATLAB software using a CLS computational method that included a broad spectral region from 2250 to 700 cm^{-1}.

The mass rate of DICDI from the first day's experiment, during which a total of 12 spectra were acquired, is shown in Figure 13. The semilog plot showed that the decay in the DICDI rate deviated somewhat from ideality. This behavior, which was also observed with VX,[12] may be related to differences in the phenomenology of the mass transport in the liquid phase between the DICDI and the lower-volatility GD. The line in the plot that connects the individual data points was therefore fitted to a second-order equation:

$$\ln(R) = 5.338 \times 10^{-6} t^2 - 0.004667(t) - 1.478 \quad (11)$$

where R represents the rate of DICDI (in $mg \cdot min^{-1}$) and t is the time (in min). The intercept in eq 11, –1.478, represents the natural logarithm of the DICDI rate at $t = 0$, and its antilog gives $R = 0.228$ $mg \cdot min^{-1}$. That value for the starting rate is less than one-half the theoretical value of $R_0 = 0.488$ $mg \cdot min^{-1}$ and may indicate that hydrogen bonding between the R–N–H of the carbodiimide and the phosphoryl (P=O) of the GD depresses the partial pressure of the DICDI. Carrier flow was maintained for a total time of 296 min. Integrating eq 11 yields

$$\int_0^{296} f(t)\mathrm{d}t = 40.8 \text{ mg} \quad (12)$$

which was the total mass of DICDI that eluted from the saturator cell during the first day's experiment. Subtracting the mass of DICDI from the total Δmass (from the gravimetric measurements) of 300.1 mg gave a Δmass of 260 mg for the GD and an average mass rate of 0.876 $mg \cdot min^{-1}$. Applying Raoult's law (eq 9) yields a predicted starting mass rate for the GD of 0.947 $mg \cdot min^{-1}$. As expected, the spectra showed little change in the regions of strong absorption from GD, in which DICDI exhibited little or no absorption (1100–900 cm^{-1}). Applying eq 10 yields R(GD) = 0.938 $mg \cdot min^{-1}$, which is only slightly lower than the Raoult's law prediction. The total Δmass rate from the gravimetric measurements was 1.013 $mg \cdot min^{-1}$ (300.1 mg/296 min). The combined data appear to show that just those two compounds, GD and DICDI, probably accounted for close to 100% of the vapor stream from the saturator cell.

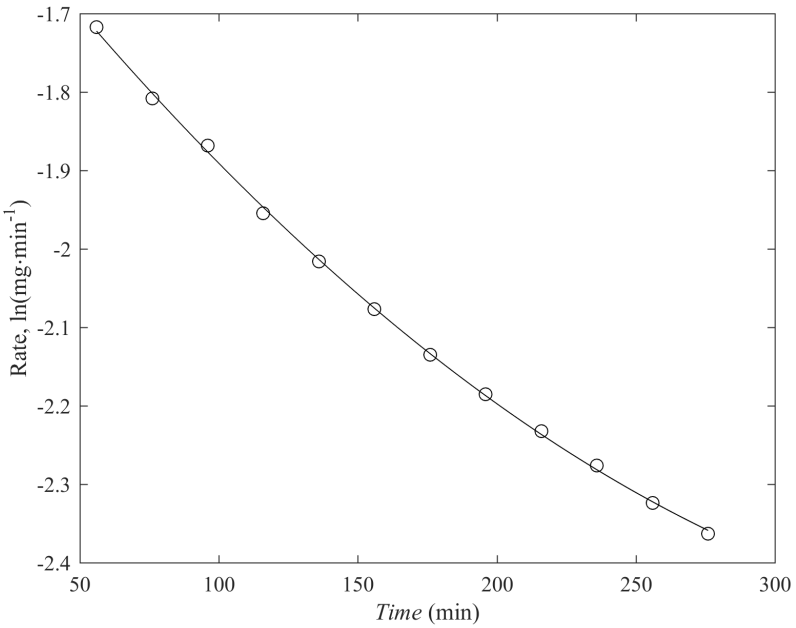

Figure 13. Mass rate of DICDI from a GD-filled saturator cell that had been spiked to a molar concentration of 3.55%. The line represents the best fit of the data points.

The GD saturator cell was run under similar conditions for nearly 19 h over a five day period. In between runs, the carrier flow was stopped, and the saturator cell was dried for several hours before it was reweighed. Prior to the next run, the saturator cell was again weighed to verify that the weight had not changed since the end of the previous run. When the DICDI mass rates from all five runs were plotted together, the DICDI decay displayed behavior similar to that observed during the analysis of weapons-grade VX.[12] As shown in Figure 14, at the beginning of each subsequent run, the mass rate of DICDI was higher than at the end of the previous run. This provided additional evidence that the mass transport of the two components in the solution, GD and DICDI, were different. An additional observation was that in the last two runs, the mass rate may have started to become asymptotic, as if the GD–DICDI system was forming an azeotrope. Overall, the data confirmed our initial observation that purging DICDI from liquid chemical agents may not be practicable.

Because the DICDI concentration in the liquid that remained in the saturator cell decreased over the course of the experiment, at least on a theoretical basis, the GD output rate should have increased. However, even after DICDI was added to the saturator cell, the molar purity of the GD (approximately 96.5%) was still very high relative to the DICDI concentration. For that reason, we did not necessarily expect to be able to detect an increase in the GD ouptut as the DICDI concentration decreased. When it was plotted, however, the GD output rate appeared to exhibit a slow increase over the course of the runs, as shown in Figure 15. The mean computed mass rate of GD (computed from the spectra) on day 5 was 1.023 $mg \cdot min^{-1}$, which was close to the predicted mass rate of pure GD under the experimental conditions, 0.982 $mg \cdot min^{-1}$. Such a close agreement was encouraging and illustrated the value of the saturator cell technique for obtaining stable, predictable streams of compounds and the usefulness of IR spectra for determining compound concentrations when absorptivity coefficients

are known. We note that we have not studied in a systematic way the uncertainties in the CLS method that was used to compute the mass rates of compound mixtures from their spectra. As an example of one factor that contributes to the overall uncertainty in such computations, the uncertainties in the reference spectra of GD that we used were 2.7% (Type A) and 3.0% (Type B).[8]

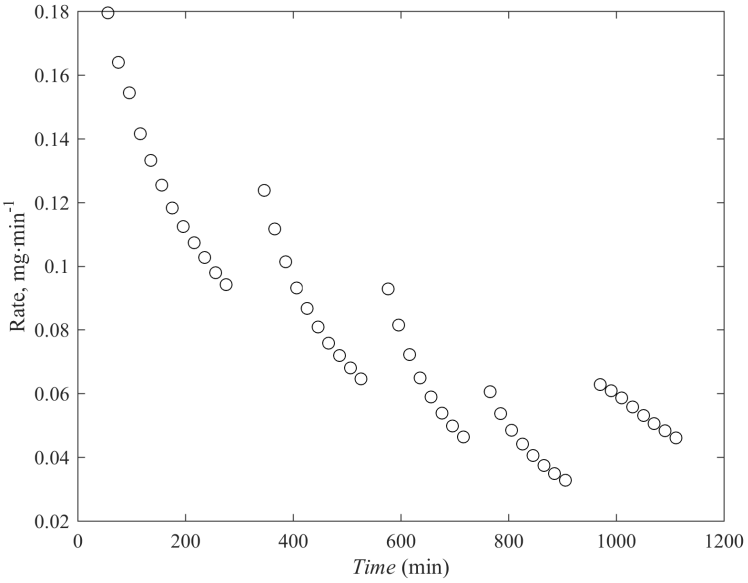

Figure 14. Mass rate of DICDI from GD-filled saturator cell that had been spiked with the stabilizer as a function of time. At the beginning of each subsequent run, the initial mass rate was higher than at the end of the previous run, which appeared to provide further evidence that the mass transport of DICDI and GD in the liquid phase differed from one another.

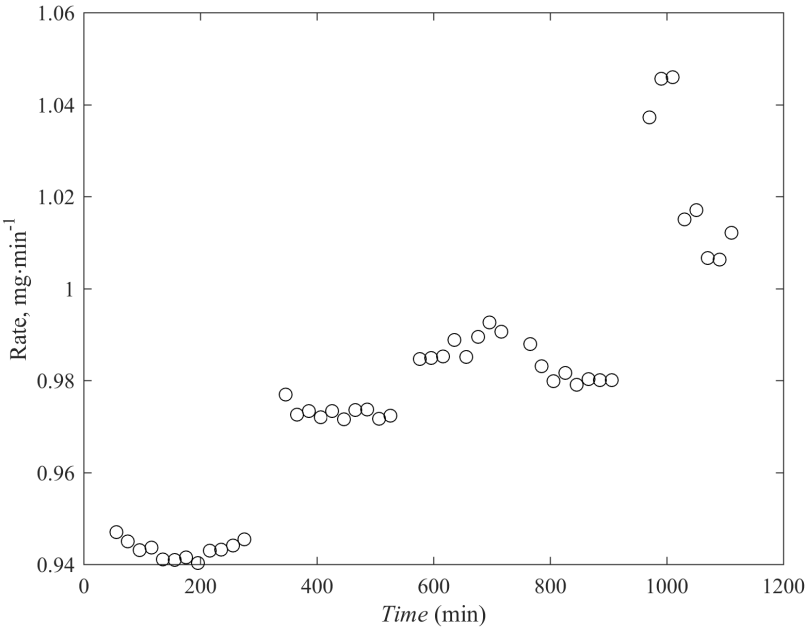

Figure 15. Mass rate of GD from saturator cell as a function of time. As the concentration of DICDI decreased, the rate of GD increased, as predicted from Raoult's law.

The conclusions from the saturator cell experiments with DICDI-stabilized GD were as follows:

- Because of the relatively high vapor pressure of DICDI, the compound contributed a much higher mass (and molar) fraction to the vapor-phase spectra of the stabilized GD than to the complex refractive index of the liquid agent.
- Although DICDI is a strong IR absorber, because its region of strongest absorption is well outside the fingerprint region, the compound had little effect on the shapes and intensities of absorption features in the fingerprint region. An impurity with a similarly high vapor pressure and absorption bands in the fingerprint region would be expected to have much larger effects on the shapes and intensities of the target chemical agent within the fingerprint region.
- The behavior of even a simple binary system, such as DICDI–GD, can at best only be approximated from first principles. Such approximations must be verified empirically.

4. CONCLUSIONS

We measured the complex optical constants ($\hat{n} = n + \mathrm{i}k$) of five lots of the nerve agent GD in the mid-infrared region, including CASARM-grade, weapons-grade, and thickened GD agent using IR ATR-VASE. Further, we systematically studied the effects of a stabilizer, DICDI, on vapor-phase spectra of GD that were generated from the GD. As expected, the stabilizer had a much larger effect on the vapor-phase than the liquid-phase spectra, although the compound had only a small effect on spectra of the agent within the fingerprint region.

Blank

LITERATURE CITED

1. Stenzel, O. *Das Dunnschichtspektrum*; Springer Verlag: Berlin, 1996.

2. Colthup, N.B.; Daly, L.H.; Wiberley, S.E. *Introduction to Infrared and Raman Spectroscopy*, 3rd ed.; Academic Press: San Diego, CA, 1990.

3. Williams, B.R.; Hulet, M.S.; Ben-David, A.; Miles, R.W.; Samuels, A.C.; Zhu, C.-J.; Green, N. *Validation and Support of a Quantitative Infrared Instrument Facility and Generation of a Library of Chemical Warfare and Related Materials by Fourier Transform Infrared Spectroscopy*; ECBC-CR-076; U.S. Army Edgewood Chemical Biological Center: Aberdeen Proving Ground, MD, 2006; UNCLASSIFIED Report (ADA471712).

4. Williams, B.R.; Samuels, A.C.; Miles, R.W.; Hulet, M.S.; Ben-David, A. ECBC Quantitative Vapor-Phase Infrared Spectral Database. In *Proceedings of the 2006 Scientific Conference on Chemical & Biological Defense Research*, 13–15 November 2006; SOAR-07-20; Hunt Valley, MD; 2007.

5. Samuels, A.C.; Miles, R.W., Jr.; Williams, B.R.; Hulet, M.S. *Vapor-Phase Infrared Absorptivity Coefficient of Cyclohexyl Isothiocyanate*; ECBC-TR-637; U.S. Army Edgewood Chemical Biological Center: Aberdeen Proving Ground, MD, 2008; UNCLASSIFIED Report (ADA485730).

6. Williams, B.R.; Hulet, M.S.; Samuels, A.C.; Miles, R.W.; Berg, F.J.; McMahon, L.; Durst H.D. *Vapor-Phase Infrared Absorptivity Coefficient of* Bis-*(2-chloroethyl) Sulfide*; ECBC-TR-638; U.S. Army Edgewood Chemical Biological Center: Aberdeen Proving Ground, MD, 2008; UNCLASSIFIED Report (ADA487002).

7. Williams, B.R.; Hulet, M.S.; Samuels, A.C.; Miles, R.W., Jr.; Berg, F.J.; McMahon, L.; Durst, H.D. *Vapor-Phase Infrared Absorptivity Coefficient of 2-Chlorovinyl Dichloroarsine (Lewisite)*; ECBC-TR-667; U.S. Army Edgewood Chemical Biological Center: Aberdeen Proving Ground, MD, 2008; UNCLASSIFIED Report (ADA493633).

8. Williams, B.R.; Hulet, M.S.; Samuels, A.C.; Miles, R.W., Jr.; *Vapor-Phase Infrared Absorptivity Coefficient of Pinacolyl Methylphosphonofluoridate*; ECBC-TR-688; U.S. Army Edgewood Chemical Biological Center: Aberdeen Proving Ground, MD, 2009; UNCLASSIFIED Report (ADA500806).

9. Williams, B.R.; Hulet, M.S.; Samuels, A.C.; Miles, R.W., Jr.; *Vapor-Phase Infrared Absorptivity Coefficient of* O,S-*Diethyl Methylphosphonothioate*; ECBC-TR-693; U.S. Army Edgewood Chemical Biological Center: Aberdeen Proving Ground, MD, 2009; UNCLASSIFIED Report (ADA501027).

10. Williams, B.R.; Hulet, M.S.; Samuels, A.C.; Miles, R.W., Jr. *Vapor-Phase Infrared Absorptivity Coefficients of Three 2-(Dialkylamino)ethanethiol Compounds*; ECBC-TR-706; U.S. Army Edgewood Chemical Biological Center: Aberdeen Proving Ground, MD, 2009; UNCLASSIFIED Report (ADA505615).

11. Williams, B.R.; Hulet, M.S.; Samuels, A.C.; Miles, R.W., Jr. *Vapor-Phase Absorptivity Coefficient of Ethyl N,N-Dimethylphosphoramidocyanidate*; ECBC-TR-732; U.S. Army Edgewood Chemical Biological Center: Aberdeen Proving Ground, MD, 2010; UNCLASSIFIED Report (ADA713632).

12. Williams, B.R.; Hulet, M.S.; Samuels, A.C.; Miles, R.W., Jr. *Vapor-Phase Infrared Spectral Study of Weapons-Grade O-Ethyl S-2-(Diisopropylamino)ethyl Methylphosphonothiolate (VX)*; ECBC-TR-955; U.S. Army Edgewood Chemical Biological Center: Aberdeen Proving Ground, MD, 2012; UNCLASSIFIED Report (ADA562293).

13. Williams, B.R.; Samuels, A.C.; Hulet, M.S.; Miles, R.W.; Ben-David, A.; Yang, C. Effects of Impurities on the Generation of Vapor-Phase Spectra of Chemical Agents in the Mid-Infrared. Presented at the Defense Threat Reduction Agency 2011 Chemical and Biological Defense Science and Technology Conference, Las Vegas, NV, 14–18 November 2011.

14. Mills, I.; Civitaš, T.; Homann, K.; Kallay, N.; Kuchitsu, K.; *Quantities, Units and Symbols in Physical Chemistry*, 2nd ed.; International Union of Pure and Applied Chemistry; Blackwell Science: Oxford, U.K., 2008.

15. Yang, C.S.C.; Samuels, A.C.; Miles, R.W., Jr.; Williams, B.R.; Hulet, M.S. *Infrared Complex Optical Constants of GB, GF, HD, HN1, and VX*; ECBC-TR-1166; U.S. Army Edgewood Chemical Biological Center: Aberdeen Proving Ground, MD, 2014; UNCLASSIFIED Report.

16. Yang, C.S.-C.; Williams, B.R.; Hulet, M.S.; Tiwald, T.E.; Miles, R.W.; Samuels, A.C. Optical Constants of Neat Liquid-Chemical Warfare Agents and Related Materials Measured by Infrared Spectroscopic Ellipsometry. In *Proceedings of SPIE 8018: Chemical, Biological, Radiological, Nuclear, and Explosives (CBRNE) Sensing XII*; presented 13 May 2011; doi: 10.1117/12.882067.

17. *Potential Military Chemical/Biological Agents and Compounds*; FM 3-11.9; Department of the Army: Washington, DC, January 2005; UNCLASSIFIED Field Manual.

18. Sharpe, S.; Johnson, T.; Sams, R.; Hylden, J.; Kleimeyer, J.; Rowland, B. Infrared Spectral Signatures: Creation of Reference Data for Vapors and Liquids. *Int. J. High Speed Electron.* **2008,** *18,* 231–250.

19. *Paraloid K-125 Processing Aid for Vinyl*; Rohm and Haas Company: Philadelphia, PA, 2006; http://www.dow.com/assets/attachments/business/plastics_additives/paraloid_k/paraloid_k-125/tds/paraloid_k-125.pdf (accessed 16 April 2019).

20. *Chemical, Biological, and Radiological Contamination Survivability: Material Effects Testing*; *Test Operating Procedure (TOP) 08-2-502;* West Desert Test Center: Dugway, UT, 2012; http://www.dtic.mil/dtic/tr/fulltext/u2/a565279.pdf (accessed 16 April 2019).

21. Armour, S.J.; Ogston, J.M.G. *The Characterization of the Simulant System, K 125/Methyl Salicylate*; Suffield Report 390; Defence Research Establishment Suffield: Ralston, Alberta, 1989; UNCLASSIFIED Report; http://cradpdf.drdc-rddc.gc.ca/PDFS/unc52/p59511.pdf (accessed 16 april 2019).

22. Pouchert, C.J. *The Aldrich Library of FT-IR Spectra;* 2nd ed.; Aldrich Chemical Company: Milwaukee, WI, 1997.

23. Yang, C.S.C; Williams, B.R.; Tripathi, A.; Hulet, M.S.; Samuels, A.C.; Domanico, J.A.; May, J.; Miles, R.W., Jr.; Fountain, A.W., III. *Spectral Characterization of RDX, ETN, PETN, TATP, HMTD, HMX, and C-4 in the Mid-Infrared Region*; ECBC-TR-1243; U.S. Army Edgewood Chemical Biological Center: Aberdeen Proving Ground, MD, 2014; UNCLASSIFIED Report.

24. *MATLAB: The Language of Technical Computing. Using MATLAB Graphics,* version 6; The Mathworks: Natick, MA, 2002.

25. Griffiths, P.R.; de Haseth, J.A. *Fourier Transform Infrared Spectrometry,* 2nd ed.; John Wiley & Sons: Hoboken, NJ, 2007.

26. Ebbing, D.D. *General Chemistry*, 2nd ed.; Houghton Mifflin: Boston, 1987.

27. Nyquist, R.A. *The Interpretation of Vapor-Phase Infrared Spectra; Vol. 1, Group Frequency Data*; Sadtler Research Laboratories: Philadelphia, PA, 1984.

28. Balboa, A.; Buchanan, J.H.; Buettner, L.C.; Sewell, T.; Tevault, D.E. *Vapor Pressure of GD*; ECBC-TR-575; U.S. Army Edgewood Chemical Biological Center: Aberdeen Proving Ground, MD, 2007; UNCLASSIFIED Report (ADA473748).

29. Brozena, A.; Williams, B.R.; Tevault, D.E. *Vapor Pressure of N,N′-Diisopropylcarbodiimide (DICDI)*; ECBC-TR-1352; U.S. Army Edgewood Chemical Biological Center: Aberdeen Proving Ground, MD, 2016; UNCLASSIFIED Report (AD1003693).

Blank

ACRONYMS AND ABBREVIATIONS

ATR-VASE	attenuated total reflection variable-angle spectral ellipsometer
CASARM	Chemical Agent Standard Analytical Reference Material
CAS RN	Chemical Abstracts Service Registry Number
CL	concentration–pathlength product
CLS	classical least squares
CoA	certificate of analysis
DICDI	diisopropylcarbodiimide
ECBC	U.S. Army Edgewood Chemical Biological Center
ED	Euclidean distance
FTIR	Fourier transform infrared
GB	isopropyl methylphosphonofluoridate, sarin
GC	gas chromatography
GD	pinacolyl methylphosphonofluoridate, soman
HQI	hit quality index
ik	imaginary refractive index
IR	infrared
IRE	internal reflection element
IUPAC	International Union of Pure and Applied Chemistry
k	absorption index
K	linear absorptivity coefficient
K–K	Kramers–Kronig
MS	mass spectrometry
ν	wavenumber
n	real part of the refractive index
NMR	nuclear magnetic resonance
PinOH	pinacolyl alcohol
PMMA	poly(methyl methacrylate)
PNNL	Pacific Northwest National Laboratory
RLS	robust least squares
rms	root mean square
TGD	thickened GD
TIC	total ion chromatogram

DISTRIBUTION LIST

The following individuals and organizations were provided with one Adobe portable document format (pdf) electronic version of this report:

U.S. Army Combat Capabilities Development
Command Chemical Biological Center
(CCDC CBC)
FCDD-CBR-PD
ATTN: Williams, B.
Morrissey, K.

CCDC CBC
Technical Library
FCDD-CBR-L
ATTN: Foppiano, S.
Stein, J.

Defense Technical Information Center
ATTN: DTIC OA


U.S. ARMY COMBAT CAPABILITIES DEVELOPMENT COMMAND
CHEMICAL BIOLOGICAL CENTER